Signal Processing 237 (2025) 110108

Contents lists available at ScienceDirect

Signal Processing

journal homepage: www.elsevier.com/locate/sigpro

WaveGRU-Net: Robust non-contact ECG reconstruction via MIMO millimeter-wave radar and multi-scale semantic analysis

Dan Xu [a,d,*], Yiming Xu [b], Kaijie Xu [c], Ze Hu [c], Mengdao Xing [a,c], Fulvio Gini [d], Maria Sabrina Greco [d]

[a] The Academy of Advanced Interdisciplinary Research, Xidian University, Xi'an 710071, PR China
[b] School of Electronics and Information, Xi'an Polytechnic University, Xi'an 710048, PR China
[c] School of Electronic Engineering, Xidian University, Xi'an 710071, PR China
[d] Department of Information Engineering University of Pisa, Pisa, Italy

ARTICLE INFO

Keywords:
Non-contact vital sign monitoring
Non-contact ECG reconstruction
MIMO millimeter-wave radar
WaveGRU-Net

ABSTRACT

With the rising demand for telemedicine, non-contact heart beating monitoring has attracted significant interest due to its non-invasive and patient-friendly attributes. However, conventional approaches are typically limited to detecting the peaks of the Electrocardiogram (ECG), making the accurate extraction of ECG intervals challenging. This paper proposed a novel method for non-contact ECG signal reconstruction utilizing multiple-input-multiple-output millimeter-wave radar, enabling precise reconstruction of comprehensive ECG features and capturing nuanced variations in cardiac activity. First, Two-Dimensional beamforming is employed to enhance the radar signal of interest. The echo inevitably contains interference from random body movements and chest displacements caused by respiration. The interference from random body movements can be effectively suppressed by using a cumulative energy spectrum analysis. Next, the phase information representing the combined respiratory and cardiac micro-movements is extracted. Then, the phase is inputted into the WaveGRU-Net model, which is an advanced neural network based on the Convolutional Neural Network-Long Short-Term Memory architecture, to reconstruct heartbeat signals and ECG waveforms. The proposed method successfully separates respiratory and cardiac signals in the time-frequency domain, yielding a refined ECG reconstruction enriched with detailed semantic features that encapsulate subtle cardiac dynamics. Experimental results demonstrate the proposed method has strong semantic representation capabilities.

1. Introduction

Heart rate, respiration, and blood pressure are key vital signs that reflect an individual's health status, with abnormalities often indicating potential health risks or emergency medical conditions [1]. Vital sign monitoring methods can be broadly divided into contact and non-contact approaches. Despite the availability of smart wearables [2], these devices may cause discomfort for certain groups of people. For instance, for burn patients, wearing the devices can irritate the injured skin, making it difficult to tolerate extended use. Additionally, privacy-conscious individuals might worry about personal data security when using these devices, affecting their willingness to engage with and trust in vital sign monitoring. This may compromise accurate measurements of heart rate, respiratory rate, and blood oxygen levels. Thus, non-contact vital sign monitoring is highly valuable for biomedical health surveillance [3–6]. Non-contact monitoring, particularly of respiration and heartbeat, relies on detecting minute physiological movements in the range of millimetres to centimetres. However, random body movements (RBM) can cause displacements as large as, or larger than, those from vital signs, introducing interference that significantly reduces the accuracy of vital sign estimation.

Non-contact vital sign monitoring technologies have advanced rapidly in recent years. Detection methods utilizing radio frequency (RF) signals [7–9] have demonstrated significant potential, enabling precise

This work was supported in part by the Fundamental Research Funds for the Central Universities under Grant ZYTS25156, in part by the National Natural Science Foundation of China under Grant 62401430, 62301389, 62101400 and 92367206..

* Corresponding author.
E-mail addresses: danxu@xidian.edu.cn (D. Xu), qiyuetuandui@163.com (Y. Xu), kjxu@xidian.edu.cn (K. Xu), zehu_mail@163.com (Z. Hu), mdx@xidian.edu.cn (M. Xing), fulvio.gini@unipi.it (F. Gini), maria.greco@unipi.it (M.S. Greco).

https://doi.org/10.1016/j.sigpro.2025.110108
Received 4 December 2024; Received in revised form 21 March 2025; Accepted 14 May 2025
Available online 15 May 2025

heartbeat detection by capturing subtle physiological movements, such as chest wall displacements. Some studies have demonstrated the potential of deep learning in radar signal processing through neural network model designs, enabling accurate extraction and prediction of vital signs [10–17]. For example, the MoVi-Fi system developed by Chen et al. allows for accurate recovery of vital sign waveforms even in the presence of significant body motion [10]. Chang et al. proposed a deep learning-assisted weighting scheme using Frequency Modulated Continuous Wave (FMCW) radar, where data fusion techniques are employed to enable rapid acquisition and high-precision estimation of vital sign signals [11]. Research on the heart's mechanical and electrical activities has also been deepening to enhance cardiac health monitoring. research on the cardiac excitation-contraction coupling (electrocardiogram, ECC) mechanism [12], along with subsequent modeling studies [13,14], has not only provided an integrated framework for understanding cardiac function by linking electrical and mechanical activities, but also revealed the mapping relationship between these two types of cardiac activity. Dong et al. verified the method's capability to translate mechanical motion into accurate temporal information for heart sounds [15]. Haescher et al. successfully converted ECG signals into seismocardiogram (SCG) signals by applying convolution to transform SCG into ECG signals [16]. This suggests the possibility of converting between different cardiac detection signals, which contain valuable cardiac information. However, the exact relationship between these signals remains not fully understood [17].

Currently, most radar-based heartbeat detection methods focus primarily on R-peak estimation. Yamamoto et al. proposed a model that utilizes convolutional Long Short-Term Memory (LSTM) networks, taking the spectrogram of radar signals as input and outputting bandpass filtered ECG signals. The model calculates the R-R interval (RRI) through peak detection [18–20]. Wu et al. employed a combined Convolutional Neural Network (CNN) and Recurrent Neural Network (RNN) model to estimate triangle waves with two maximum-matching R and S peaks from radar signals [21,22]. While these methods can detect heartbeat intervals, they reduce the detailed features of ECG signals, limiting their suitability for advanced feature extraction where detailed heartbeat information is required [23] and [24] have employed CNN and CNN+LSTM architectures to reconstruct ECG signals from radar data. However, the quality of the reconstructed signal is often affected by the input signal quality and the limitations of the network architecture. To address these issues, some studies have adopted alternative approaches. Zhi et al. extracted features from the amplitude and phase of UWB signals and combine them in a latent space [25]. Dong et al. mapped extracted features into a latent space to reconstruct SCG signals by using CNN for template matching and U-net for annotating key cardiac events like valve movements and isovolumetric contraction [26]. Shanling et al. proposed a model that extracts features using bimodal Gaussian distribution and Shannon energy, and identifies key waveforms through K-means clustering. The model further segments rhythm sequences with RNN, enabling precise detection of cardiac contraction and relaxation states [27].

Current methods can identify basic features of heartbeat signals, but the reconstructed ECG signals contain limited semantic information across different time intervals. This limitation complicates the extraction of precise cardiac motion information from high-noise reflection signals. In addition, the large input dimensions required by high-frequency radar sampling in deep learning, along with the need to model redundant spatial and long-duration signals, further complicate the issue. These factors collectively impact ECG signal extraction and reconstruction, making high-precision ECG signal reconstruction a challenging task.

For an ECG, the QRS complex is an important parameter, and its shape and duration can reflect the health of the ventricles. Inspired by the R and S peak template matching approach in [21] and the CNN-based template matching strategy in [22], this study utilizes millimeter-wave FMCW radar to design the WaveGRU-Net network model, integrating a CNN-LSTM architecture for enhanced performance. The goal is to reconstruct ECG signals by analyzing temporal features in radar signals. This model integrates maximal overlap discrete wavelet transform (MODWT) for signal denoising and employs a multi-layer CNN to perform template matching on four ECG intervals: R-R interval, P-R interval, Q-T interval, and QRS complex. By tuning the number of CNN layers, we effectively extract temporal features from the signal, while the bidirectional GRU (Bi-GRU) captures long-term dependencies, enabling efficient reconstruction of complex time-series characteristics in ECG signals. To validate the effectiveness of the algorithm, we conduct multiple real-world experiments and compare the proposed approach with the traditional CNN-LSTM network [24,28]. The results indicate that the reconstructed ECG signals using the proposed method exhibit greater morphological consistency with real ECG signals. The reconstructed ECG signals are evaluated for the four major ECG intervals—R-R, P-R, Q-T, and QRS—and short-term variability is quantified using the root mean square of successive differences (RMSSD) between heartbeats. Additionally, the standard deviation of IBI values (SDRR) and the pNN50 methods are applied to validate the heart rate variability (HRV) in the inter-beat interval (IBI), ensuring the reliability of the semantic information in the reconstructed ECG signals.

The structure of this paper is organized as follows: Section II establishes the heartbeat signal model under millimeter-wave radar observation. Section III introduces the ECG reconstruction method based on WaveGRU-Net, including millimeter-wave radar data preprocessing and the MODWT-CNN-BiGRU architecture. Section IV conducts experiments on real-world data, comparing the proposed algorithm with existing methods. It evaluates the consistency and accuracy of ECG reconstruction, demonstrating the effectiveness and superiority of the proposed algorithm. Finally, Section V summarizes the proposed algorithm and discusses potential future research directions.

2. Radar signal modeling of heartbeat

The generation of an ECG begins with the heart's electrical activity, originating in the sinoatrial (SA) node. Pacemaker cells within the SA node spontaneously generate electrical signals, initiating atrial depolarisation, which produces the P-wave, signifying atrial contraction. The electrical signal then passes through the atrioventricular (AV) node to the ventricles, where it propagates along the Bundle of His, left and right bundle branches, and Purkinje fibres, triggering ventricular depolarisation. This process forms the QRS complex, indicating a forceful ventricular contraction. Following depolarisation, the ventricles repolarise, producing the T-wave, which marks the relaxation phase as the heart prepares for the next contraction. The resulting electrical activity initiates mechanical motion, which ensures the rhythmic pumping of blood by the heart. Cardiac mechanical activity, such as ventricular contraction, not only propels blood flow but also vibrates the chest cavity to produce heart sounds, notably the S1 and S2 sounds generated during ventricular closure [15,29]. Various technologies have been developed to study these movements, including tagged magnetic resonance imaging (MRI) [30], tissue Doppler imaging (TDI) [31], speckle-tracking imaging (STI) [32], Seismocardiography (SCG) [33], and Gyrocardiography (GCG) [34]. Based on the above analysis, this paper proposes a non-contact ECG signal reconstruction method using MIMO millimeter-wave radar, which can accurately reconstruct key ECG features and effectively capture semantic information related to subtle cardiac activity changes.

Fig. 1

Millimeter-wave radar detects subtle cardiac motions by measuring phase variations in reflected signals. These variations result from displacements caused by the expansion and contraction of the chest cavity, thereby reflecting the mechanical activity induced by cardiac electrical signals. Generally, during millimeter-wave radar observations, the individual remains in a quasi-static state. This study employs a radar system with a 3-transmit and 4-receive antenna configuration, utilizing

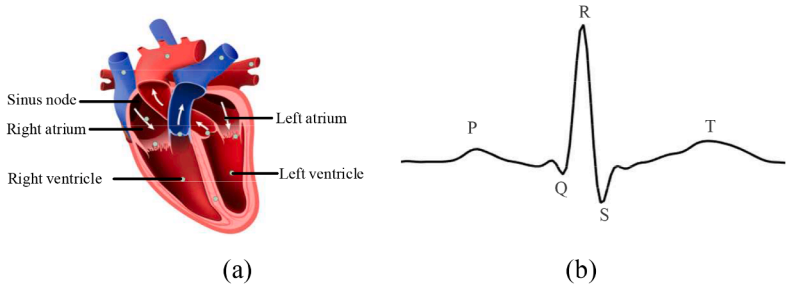

Fig. 1. The Heart and the ECG structure. (a) Cardiac structure. (b) ECG structure.

Time Division Multiplexing-MIMO technology for signal acquisition, as shown in Fig. 2(a). Fig. 2(b) illustrates the layout of the transmitting and receiving antennas. The four receiving antennas, along with transmit antennas 1 and 3, are aligned on the same horizontal line, with a spacing of half a wavelength between the receiving antennas. The three transmitting antennas are arranged one wavelength apart, with transmit antenna 2 positioned half a wavelength above the horizontal line. Such a layout can enhance the spatial resolution of the signal.

The transmitting antennas operate sequentially according to a set time schedule. Assume that the transmitted linear frequency-modulated signal is $s_t(t)$, then

$$s_t(t_f) = A_t \exp\{j(2\pi f_c t_f + \pi\beta t_f^2)\} \tag{1}$$

where A_t is the amplitude of the transmitted signal, f_c represents the carrier frequency, β is the chirp rate, and t_f is the fast time. The signal contains vibrations caused by the heartbeat, chest expansion and contraction due to breathing, as well as random body tremors [35]. Considering that the heartbeat frequency is much lower than the sampling rate in the fast time dimension, a "Step-and-Stare" mode is adopted. Therefore, the distance between the target and the radar can be expressed as

$$d(t_m) = d_0 + r(t_m) \tag{2}$$

$$r(t_m) = A_h \sin(2\pi f_h t_m + \varphi_h) + A_b \sin(2\pi f_b t_m + \varphi_b) + \sigma W_t(t_m) \tag{3}$$

where is the slow time, A_b is the $t_m$amplitude of the heartbeat, f_b is the heartbeat frequency, φ_b is the initial phase of the heartbeat, A_h is the amplitude of respiration, f_h is the respiration frequency, φ_h is the initial phase of respiration, $d_0$is the average distance between the radar and the human body, σ represents the amplitude of Gaussian white noise, W_t denotes the distribution of Gaussian white noise. For a single channel, the received signal $s_r(t_m)$ is

$$s_r(f, t_m) = A_r \exp\left\{-j\frac{4\pi}{c}(f_c + f)d(t_m)\right\} \tag{4}$$

where A_r denotes the amplitude of the received signal, f denotes fast time frequency, and c denotes the speed of light. For MIMO radar, we recorded the IQ signal immediately after the ADC and reorganized it into a four-dimensional complex-valued matrix with the structure Rx antennas, frames, chirps, and samples. To ensure uniformly spaced points in the time dimension spanning both the frames and chirps dimensions, we retained only the first chirp of each frame, eliminating the apparent gaps between chirps caused by the inter-frame time. This reduction resulted in a three-dimensional matrix for processing, where the samples dimension represents the fast-time domain, and the frames dimension corresponds to the slow-time domain [44]. Therefore, the signal data cube can be represented as

$$s(t_f, t_m, l) = A_r \exp\left\{j\left(2\pi f_c\left(t_f - \frac{2d(t_m)}{c}\right) + \pi\beta\left(t_f - \frac{2d(t_m)}{c}\right)^2 + \phi_l\right)\right\} \tag{5}$$

$$\phi_l = \frac{2\pi}{\lambda}(x_l \sin\varphi\cos\theta + y_l \sin\varphi\sin\theta) \tag{6}$$

where ϕ_l denotes the phase offset of the antenna channel, (x_l, y_l) represents the coordinates of the lth receiving channel, θ is the azimuth angle of the target, and φ is the elevation angle of the target.

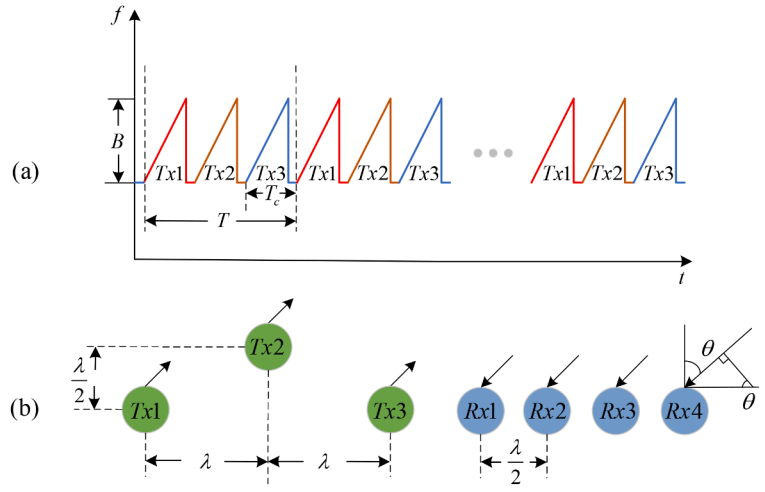

Fig. 2. Millimeter-wave radar system antenna configuration: (a) Time-division multiplexing (TDM) signal transmission scheme, (b) MIMO antenna array arrangement.

3. ECG reconstruction based on WaveGRU-net

The moving target indication (MTI) algorithm is first applied to remove static background interference, retaining only dynamic signals reflected by the human body [36–38]. Next, a Two-Dimensional (2D) beamforming technique is used to focus on the target signal at specified elevation and azimuth angles. The sliding window method is then applied to precisely lock onto the target range cell and isolate the target signal. Phase unwrapping is used to eliminate phase ambiguity caused by periodic phase shifts, ensuring the continuity of phase. MODWT is used for denoising, while CNN utilizes ECG interval features for template-based temporal feature extraction. Bi-GRU captures long-term dependencies, enhancing the network's ability to map radar signals to ECG. This approach enables high-precision ECG reconstruction. The flowchart of the proposed algorithm is shown in Fig. 3.

3.1. Radar signal preprocessing

The overall flowchart of the radar signal preprocessing is shown in Fig. 4. To capture the complete cardiac transmission motion, it is necessary to focus on periodic signals associated with cardiac activity. First, the three-dimensional (3D) data cube should be converted into a 2D matrix format. Assume that the sampling number is N_f in fast time with a sampling interval of Δt_f, $t_f = n{\cdot}\Delta t_f$, where $n = 0,1,\ldots,N_f - 1$. The number of samples is N_m in slow time with a sampling interval of Δt_m, $t_m = m{\cdot}\Delta t_m$, where $m = 0,1,\ldots,N_m - 1$. The received 3D signal matrix is:

$$s(n,m,l) = A_{IF}\exp\left\{j\left(2\pi f_c\left(n{\cdot}\Delta t_f - \frac{2d(m{\cdot}\Delta t_m)}{c}\right) + \phi_l\right)\right\} \tag{7}$$

Then, the fast-time dimension is converted through the Fourier transform with respect to n to obtain:

$$S(k,m,l) = \sum_{n=0}^{N_f-1} s(n,m){\cdot}\exp\left(-j{\cdot}2\pi{\cdot}\frac{k{\cdot}n}{N_f}\right) \tag{8}$$

where $k$is the range dimension index. Since the received signal contains information about the entire scene, a MTI filter is applied along the slow-time dimension to suppress static clutter and enhance moving components. Therefore, we have

$$S_{\mathrm{MTI}}(k,m,l) = S(k,m+1,l) - S(k,m,l) \tag{9}$$

Digital beamforming (DBF) transforms the three-dimensional radar data into a two-dimensional representation by coherently combining signals across the channel dimension. This process applies phase shifting and weighting to enhance the desired signal while suppressing interference [39]. By aligning the signals in phase, DBF reduces data dimensionality while preserving key range and Doppler information for further processing. The electromagnetic echo from the heartbeat is relatively weak. After 2D beamforming, the signal from target's direction is enhanced, expressed as

$$y(k,m) = \sum_{l=0}^{L-1} S_{\mathrm{MTI}}(k,m,l){\cdot}w_l{\cdot}\exp\left\{-j\frac{2\pi}{\lambda}d_n(x_l\sin\varphi_b\cos\theta_b + y_l\sin\varphi_b\sin\theta_b)\right\} \tag{10}$$

where L is the number of receiving antennas, w_l is the weighting factor for the lth channel used to adjust the phase of the signal received from each channel, λ is the wavelength of the signal, and d_n is the distance between the lth channel and the reference point. θ_b and φ_b represent the azimuth and elevation angles focused by the 2D beamformer. Additionally, different devices may have hardware discrepancies, and Nn ar least squares optimization can be applied to adjust the bias and eliminate fixed shifts in the signal, achieving direct current (DC) offset correction. After performing pulse compression and envelope alignment on the rearranged signal, the signal from target area is extracted. It then undergoes range-direction integration. The resulting 1D signal is denoted as

$$y(m) = A_r\exp\left\{-j\frac{4\pi}{c}f_c r(t_m)\right\} \tag{11}$$

Then, we extract the phase, perform phase unwrapping, and convert it into the time domain for further processing. The signal phase can be expressed as:

$$\Theta(m) = \frac{4\pi}{c}f_c r(t_m) \tag{12}$$

3.2. ECG signal reconstruction based on WaveGRU-net model architecture

Using millimeter-wave radar for non-contact heartbeat detection does not require an extended sampling duration. Generally, 5 s, equivalent to five heartbeat cycles, is sufficient. For time-series signal reconstruction, commonly used models include Bidirectional GRU (BiGRU), Bidirectional LSTM (BiLSTM), and LSTM. BiGRU is a bidirectional extension of GRU, featuring two gates, namely update and reset gates, and maintaining only a hidden state instead of a separate cell state. Compared to BiLSTM, this reduces computational complexity, making BiGRU more suitable for real-time applications and medium-length sequences, such as ECG reconstruction over a few heartbeat cycles. BiLSTM, on the other hand, retains an additional cell state, allowing it to better capture long-term dependencies. While this can be beneficial for longer ECG sequences or extended HRV analysis, it also increases computational cost and memory usage. LSTM is inherently unidirectional, meaning it can only utilize past information, whereas BiGRU and BiLSTM process both past and future information simultaneously. Given the quasi-periodic nature of ECG signals, bidirectional architectures generally outperform unidirectional models, as they leverage both preceding and succeeding data points.

Based on the above analysis, BiGRU is chosen in WaveGRU-Net because it strikes a balance between computational efficiency and modeling capability, making it well-suited for short-to-medium-length ECG sequences while still benefiting from bidirectional processing

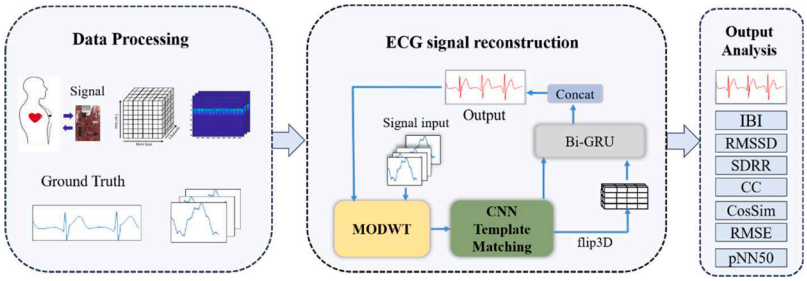

Fig. 3. The overall flowchart of non-contact ECG signal reconstruction based on MIMO radar.

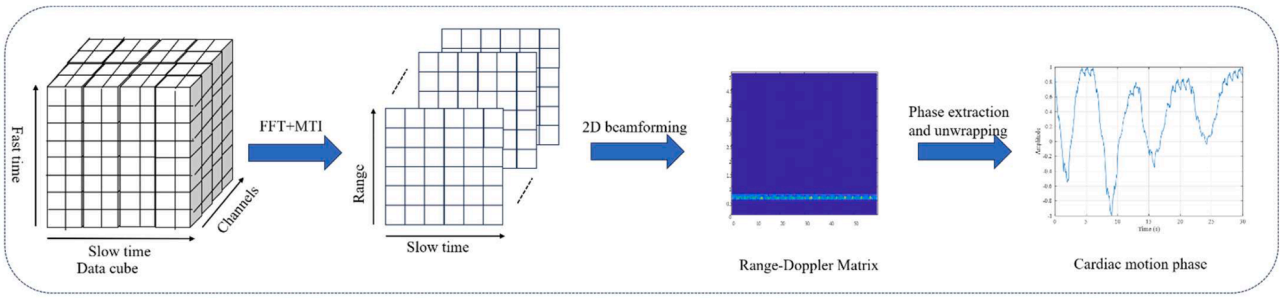

Fig. 4. Radar signal preprocessing.

advantages.

Therefore, the proposed WaveGRU-Net integrates MODWT, CNN, and Bi-GRU, as illustrated in Fig. 5. The WaveGRU-Net architecture starts with the MODWT block performing multi-scale analysis to extract essential features from the signal, enhancing frequency resolution by isolating distinct frequency bands characteristic of the ECG. Subsequently, a three-layer CNN sequentially extracts localized features of the ECG signal, with a focus on key waveforms such as the P-wave and QRS complex wave group. Finally, the Bi-GRU captures bidirectional temporal dependencies within the ECG signal, enhancing network ability to model sequential relationships embedded in the cardiac cycle.

3.2.1. *Maximal overlap discrete wavelet transform*

In this section, the raw echo signal data is processed to extract phase information related to cardiac activity. To preserve signal integrity and minimize information loss, MODWT is applied, as illustrated in Fig. 5. As an extension of discrete wavelet transform (DWT) [40], MODWT improves time-frequency resolution through overlapping sampling and removes constraints on signal length. Unlike DWT, MODWT maintains shift invariance, making it ideal for multi-scale decomposition, signal translation, denoising, and feature extraction. It has been widely utilized in speech processing, image denoising, and biomedical signal analysis [41].

Given its shift invariance and ability to handle non-stationary signals, Symlet 4 (Sym4) was chosen as the wavelet basis, with the signal decomposed into five levels. Sym4 sensitivity to abrupt changes and effective boundary handling makes it particularly suited for biomedical signal processing. MODWT ensures signal integrity across different decomposition scales while effectively reducing noise and external interference.

Beyond decomposition, MODWT enables accurate signal reconstruction, crucial for ECG signals rich in low-frequency components. By precisely isolating these components, MODWT minimizes nonlinear interference, preserving signal fidelity. Compared to other transformation methods, MODWT excels in processing stable physiological signals and is widely applied in time-frequency analysis. In this study, MODWT is employed for ECG reconstruction, performing multi-resolution analysis to extract cardiac information from the low-frequency band.

3.2.2. *CNN and Bi-GRU ECG reconstruction module*

After the MODWT layer, a CNN-based template matching method is applied to extract different interval features of the ECG, and a Bi-GRU is used to capture bidirectional temporal dependencies, enabling accurate ECG signal reconstruction. As illustrated in Fig. 5, the CNN template matching section employs a three-layer convolutional block structure, where each block consists of a conv1d layer, batch normalization (BN), a tanh activation function, and max pooling. Considering the various waveform lengths and frequency characteristics of ECG signals, along with the importance of kernel size and receptive field in capturing these features [42,43], this study progressively reduces the convolutional kernel size across layers, targeting different features to optimize extraction. The first convolutional block employs larger kernels, with 12 kernels of size 64, to capture the low-frequency, longer-duration features of signals such as the P wave, which lasts from 0.08 to 0.10 s, and the PR interval, which spans from 0.12 to 0.20 s. This ensures that these global patterns and low-frequency characteristics are preserved while minimizing noise. In the second layer, smaller kernels, with 8 kernels of size 64, are used to capture the high-frequency, rapid transitions of the QRS complex, which usually lasts from 0.06 to 0.12 s. The smaller kernel size is beneficial for isolating these brief, detailed signal elements. The third convolutional block further reduces the kernel size, with 8 kernels of size 16, to eliminate residual noise while preserving fine-grained signal features. This layer enhances the model ability to extract distinct waveform features across different ECG intervals while reducing noise interference, thereby improving both accuracy and robustness. After extracting compressed features such as the P wave and QRS complex through convolution and pooling, the signal is upsampled. It is then reconstructed using a three-layer module consisting of transposed convolution (TransConv) layers and Tanh activation functions. This process restores spatial resolution, preserves complex ECG characteristics, and enhances the overall quality of the reconstructed signal.

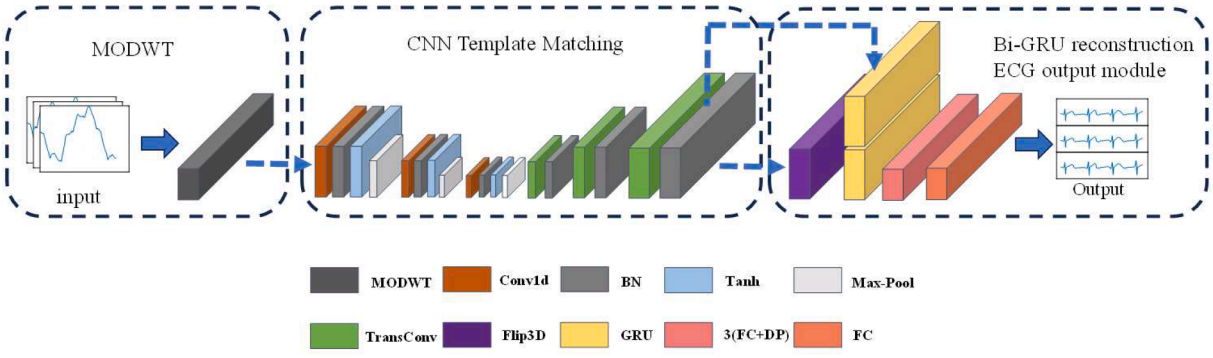

Fig. 5. Structure diagram of WaveGRU-Net.

As shown in Fig. 5, since the electrical activity of each heartbeat is closely related to the rhythm of the subsequent heartbeat, the temporal dependencies in the ECG signal are particularly considered in the ECG output module. Using the Bi-GRU structure, the input ECG signal at each time step is divided into two paths: a forward path that processes the sequence chronologically, and a reverse path, where the sequence is flipped through the Flip3D layer. This dual processing captures the cyclic dependencies in the ECG signal by analyzing both forward and backward temporal sequences. The depolarization and repolarization of each heartbeat not only in fluence the current waveform, but also connect with the subsequent cardiac electrical activity. These latent temporal dependencies are essential for identifying arrhythmias. The Bi-GRU design enhances the model's ability to capture temporal dynamics in ECG signals and, through the concat layer, merges the forward and backward features to provide complete temporal information. This is followed by multiple fully connected layers that further extract high-dimensional features, with dropout layers included to prevent overfitting and ensure the model's generalization to new data. The final output is a reconstructed ECG signal, as illustrated in Fig. 5.

4. Experimental measurement and analysis

Hardware implementation: a non-contact ECG monitoring system was developed using TI's AWR1843BOOST millimeter-wave radar system and the DCA1000 data capture board. The radar system uses three transmitters (Tx) and four receivers (Rx) to form a 12-channel virtual 2D antenna array. The transmitters sequentially emit RF signals with a 5ms interval using a time-division multiplexing strategy, capturing the baseband signal at each receiver. The system parameters are shown in the Table I.

During data collection, participants could choose to lie down or sit still, maintaining a quasi-stationary state to closely simulate typical application scenarios, such as hospital ECG monitoring or a driver's seated posture, as shown in Fig. 6. The millimeter-wave radar was positioned in front of the participant, with the antenna directed toward the chest. Since heartbeat signals are inherently weak, increasing the detection distance leads to significant signal attenuation and reduced angular resolution, degrading target signal detection capabilities. On the other hand, excessively short distances may introduce near-field effects, impacting spatial resolution. To achieve an optimal balance between signal strength, physiological signal clarity, and practical applicability in medical monitoring and driver health detection, a distance range of 0.4 to 0.7 m is commonly adopted [44,45]. During the experiment, the BMD101 device was used to collect single-lead ECG signals from the test subject. The recorded signals served as the ground truth for ECG reconstruction using the millimeter-wave radar in this study. Due to experimental constraints, the amount of collected data was not very large. A total of 40 experiments were conducted with 20 participants aged 18 to 65, including 14 males and 6 females. All participants provided informed consent. Each experiment lasted 2 min. The millimeter-wave radar had a sampling rate of 200 Hz, while the original sampling rate of the BMD101 device, used for training the WaveGRU-Net model, was 512 Hz. To ensure data consistency, the BMD101 sampling results were resampled to match the 200 Hz frequency.

Table I
Parameters setting of radar chirps and frame.

Parameter	Value
Start frequency	77 GHz
Frequency slope	65 MHz/ms
Idle time	10 ms
Ramp end time	60 ms
Sample points	256
Sample rate	5 MHz
Frame periodicity	5 ms

Data Augmentation: Due to the limited number of experimental samples, the model may suffer from overfitting during training. Therefore, data augmentation is necessary to ensure that the model can sufficiently capture heartbeat cycle signals, thereby improving its ability to learn both the regularity and abnormal variations of heartbeat signals. First, each dataset undergoes preprocessing to remove the initial unstable time segment. Then, a sliding window segmentation is applied to the 40 datasets, with a window length of 1024 samples and an overlap of 512 samples. The window length of 1024 samples corresponds to 5.12 s, which typically includes approximately five heartbeat cycles. Through data augmentation, each data segment contains sufficient heartbeat information, helping the model learn and generalize more effectively.

Software implementation: For WaveGRU-Net training, each dataset was divided chronologically, with the first 60% used for training, 20 % for validation, and the remaining 20 % for testing. The input data slices were sized at 1×1024, and the MODWT layer used the Sym4 wavelet, decomposing the signal into 5 levels across 6 layers, with an output length of 1×1024. The Adam optimizer was used, with a maximum of 800 epochs, a batch size of 900, an initial learning rate of 0.001, validation every 40 iterations, detailed logging every 40 iterations, data shuffling after each epoch, and saving the model with the best validation results. In this study, we compared two different models: (1) a traditional CNN combined with Long Short-Term Memory (LSTM), and (2) the WaveGRU-Net model, which integrates multi-level discrete wavelet transform, CNN, and GRU.

4.1. Consistency of reconstructed ECG

To evaluate the reconstructed ECG signals, we assessed system performance in terms of waveform consistency. The following metrics were used to quantify the morphological similarity between the reconstructed ECG signals and the true ECG signals. Let $X_i$and $Y_i$denote the observed values of the reference ECG signal and the reconstructed ECG signal, $\overline{X}$and $\overline{Y}$represent their respective means, and$n$ is the number of samples. The following are several evaluation metrics.

The Pearson Correlation Coefficient (PCC) is used to measure the linear relationship between two variables. The value of PCC ranges from -1 to 1, where 1 indicates a perfect positive correlation, -1 indicates a perfect negative correlation, and 0 indicates no correlation. In this evaluation, PCC is used to assess the linear dependence between the reconstructed waveform and the true waveform [23]:

$$PCC = \frac{\sum_{i=1}^{n}(X_i-\overline{X})(Y_i-\overline{Y})}{\sqrt{\sum_{i=1}^{n}(X_i-\overline{X})^2}\cdot\sqrt{\sum_{i=1}^{n}(Y_i-\overline{Y})^2}} \tag{13}$$

The Cosine Similarity (CosSim) is used to assess the similarity between two vectors. The reconstructed heartbeat waveform and the true waveform are treated as two vectors, and their cosine similarity is calculated. This metric evaluates the morphological similarity between the reconstructed waveform and the true waveform [10]:

$$CosSim = \frac{X_i\cdot Y_i}{\|X_i\|\|Y_i\|} \tag{14}$$

The Root Mean Square Error (RMSE) is used to assess the overall amplitude deviation between the reconstructed waveform and the true waveform. It represents the root mean square of errors at all time points, reflecting the differences between the reconstructed waveform and the true waveform. A smaller RMSE indicates a higher similarity between the reconstructed waveform and the true waveform, with smaller overall differences [4]:

$$\mathrm{RMSE} = \sqrt{\frac{1}{n}\sum_{i=1}^{n}(X_i-Y_i)^2} \tag{15}$$

Fig. 6. Data Collection scenarios. (a) Medical monitoring scenario. (b) Driver health monitoring scenario.

In addition, the statistical results of the experiments in this study are represented using box plots, as this method effectively visualizes the distribution, variability, and potential outliers in the data, providing a clear and intuitive comparison of different conditions. It consists of several key components: The box represents the interquartile range, which spans from the first quartile to the third quartile and covers the middle 50% of the data. Within the box, the median is marked by a horizontal line, indicating the central tendency of the data. The whiskers extend from the edges of the box to the smallest and largest values within 1.5 times the interquartile range, reflecting the overall spread of the data. Data points beyond this range are considered outliers and are typically represented by individual markers. A larger box indicates greater variability in the dataset, while a smaller box suggests more consistent values. The median position within the box provides insight into skewness. If it is centered, the data is symmetrically distributed, whereas a median closer to one end suggests a skewed distribution. The length of the whiskers indicates the range of the data, and an imbalance in their length implies asymmetry in the distribution. Outliers signal potential anomalies or variations that may require further investigation. By examining these aspects, a box plot provides a comprehensive summary of a dataset distribution and helps identify trends, patterns, and potential inconsistencies.

The performance of the WaveGRU-Net and CNN+LSTM models is illustrated in Fig. 7, evaluated through RMSE, PCC, and Cosine Similarity (CosSim). As shown in Fig. 7(a), the WaveGRU-Net model exhibits a relatively low RMSE, with values ranging from 0.05 to 0.15 and a median near 0.1, reflecting minimal and consistent reconstruction error. Both the PCC and CosSim values for WaveGRU-Net are close to 1, with the interquartile range spanning from 0.9 to 0.95, showing high consistency in waveform reconstruction with minimal outliers. In comparison, as shown in Fig. 7(b), the CNN+LSTM model demonstrates higher RMSE values, ranging from 0.1 to 0.2, with a median of approximately 0.15, indicating larger reconstruction errors and greater variability. Although the average PCC and CosSim values for CNN+LSTM are also close to 0.9, the PCC box plot reveals significant outliers, particularly near the lower limit of 0.8, and one outlier even drops below 0, suggesting issues with waveform consistency. Additionally, the CosSim metric for CNN+LSTM includes an outlier around 0.7, indicating that the reconstructed waveform deviates considerably from the true waveform in certain cases, which compromises the model stability. These results underscore the superior performance of WaveGRU-Net in terms of precision, stability, and consistency, with more accurate and reliable waveform reconstructions across all evaluation metrics. The ECG signal reconstruction results using WaveGRU-Net and CNN+LSTM are presented in Fig. 8, where the orange solid line represents the reconstructed ECG signal, and the blue dashed line represents the real ECG signal. Notably, both the real and reconstructed ECG signals have been amplitude-normalized. The results indicate that WaveGRU-Net achieves superior reconstruction accuracy. In contrast, CNN+LSTM shows noticeable deviations across multiple segments, particularly in amplitude and waveform shape. Overall, WaveGRU-Net surpasses CNN+LSTM in reconstruction quality, effectively capturing the key features of the ECG signal.

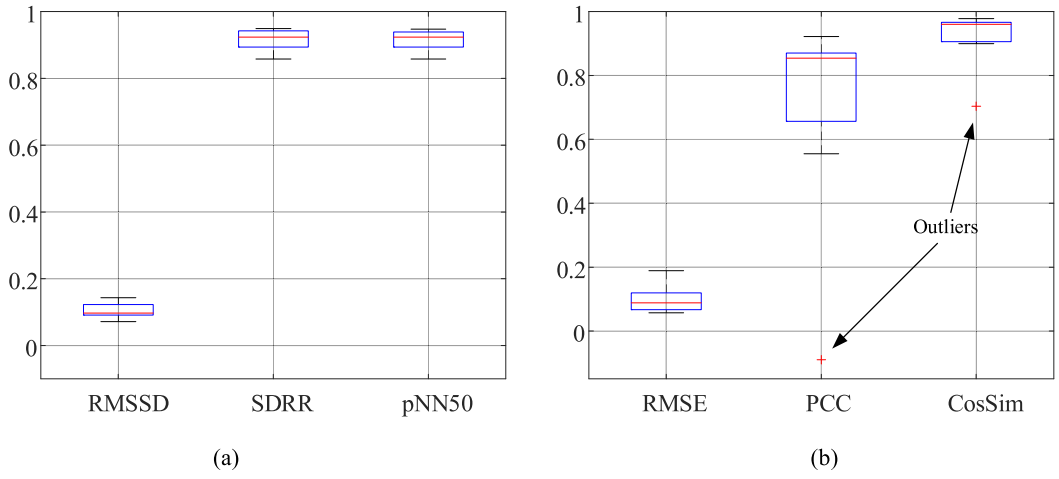

Fig. 7. Evaluation of various metrics in the experimental results of the two algorithms: (a) WaveGRU-net. (b) CNN+LSTM.

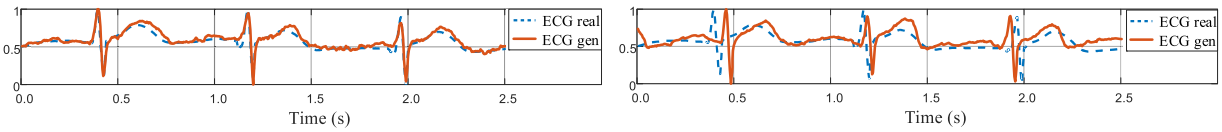

Fig. 8. Reconstructed ECG Signal by (a) WaveGRU-Net, and (b) CNN+LSTM Frame.

4.2. Evaluation of ECG reconstruction accuracy

To enhance the understanding of the experimental analysis in this section, a brief introduction to key ECG parameters is provided, as shown in Fig. 9. The R peak is the highest positive wave, and a lower amplitude may indicate heart failure or pericardial effusion. In the figure, it is marked with a triangle. The P wave is the first waveform in an ECG, typically appearing as a smooth, rounded, small positive wave before the QRS complex. Its shape and duration variations can be used to assess atrial function and cardiac rhythm. It is marked with a circle. The Q wave and S wave are the first and last negative deflections of the QRS complex in an ECG, appearing before and after the R peak, respectively. Abnormalities in their shape, such as widening or deepening, may indicate myocardial infarction or abnormal ventricular activation. In the figure, the Q wave is marked with a square, and the S wave is marked with a diamond. The T wave appears after the QRS complex and is typically a smooth, slightly symmetrical positive wave. Abnormalities in its shape may indicate myocardial ischemia or ventricular repolarization disorders. In the figure, it is marked with a star. In an ECG, the R-R, Q-T, P-R, and QRS intervals represent different phases of the heart electrical activity and serve as key indicators for evaluating heart rhythm and conduction function. The R-R interval measures the time between two consecutive R peaks, helping to calculate heart rate, with irregularities potentially indicating arrhythmias. The Q-T interval, spanning from the beginning of the Q wave to the end of the T wave, can signal an increased risk of arrhythmias if prolonged. The P-R interval, extending from the start of the P wave to the beginning of the QRS complex, reflects atrioventricular conduction time, where deviations—either too long or too short—suggest potential abnormalities in cardiac activity. The QRS interval represents the duration of the QRS complex, corresponding to ventricular depolarization. These interval parameters are crucial in ECG analysis, aiding in the detection of cardiac rhythm abnormalities, conduction disorders, and electrical activity disturbances. Therefore, this paper uses these four intervals along with key positions to evaluate the accuracy of the proposed algorithm.

Additionally, to assess the authenticity of the reconstructed signals, RMSSD, SDRR, and pNN50 are used to analyze the inter-beat interval (IBI) error and heart rate variability (HRV) specifically for the R-R interval [46]. The explanation is provided in Table II. Based on the above analysis, this paper conducts experiments using WaveGRU-Net and CNN+LSTM, evaluating the reconstructed ECG signals with the aforementioned metrics. A comparison of the interval errors for both algorithms is presented in Fig. 10 to Fig. 12.

This section evaluated 10 test subjects and compared the performance of WaveGRU-Net and CNN+LSTM in reconstruction heartbeat waveforms. Fig. 10 to Fig. 11 show the estimated relative error results of these two methods for the four ECG intervals: R-R, QRS, P-R, and Q-T. Fig. 12 further presents the average error values for these intervals. For the R-R interval, WaveGRU-Net achieved an average error of 5 ms, whereas CNN+LSTM showed a higher error of 24.5 ms, demonstrating a clear advantage for WaveGRU-Net. Similarly, for the Q-T interval, WaveGRU-Net had an average error of 5 ms, while CNN+LSTM showed an error of 24.5 ms. The P-R interval showed relatively larger errors overall, with WaveGRU-Net averaging an error of 12.25 ms, while CNN+LSTM achieved a lower error of 4.25 ms. For the QRS interval, WaveGRU-Net had an average error of 10.25 ms, while CNN+LSTM exhibited a significantly higher error of 62.5 ms, indicating considerable variability. Overall, WaveGRU-Net demonstrated consistent reconstruction with low errors for the R-R and Q-T intervals, indicating high accuracy. In contrast, CNN+LSTM exhibited significantly larger errors for the QRS interval, suggesting a less reliable performance in capturing the critical interval.

For HRV analysis on the ten sets of test data, we used the common metrics RMSSD, SDRR, and pNN50 to evaluate the variability in inter-beat intervals, which reflects both short-term and long-term heart rate

Table II
The explanation of Interval error, RMSSD, SDRR, and pNN50.

Metrics	Explanations
Interval error	Defined as the time difference between the reconstructed ECG intervals and the true ECG intervals.
RMSSD	The root mean square of successive differences between inter-beat intervals, commonly used to quantify HRV.
SDRR	The standard deviation of all IBI values, used to assess IBI variability.
pNN50	The percentage of successive IBIs that differ by more than 50 ms, also commonly used as an HRV indicator.

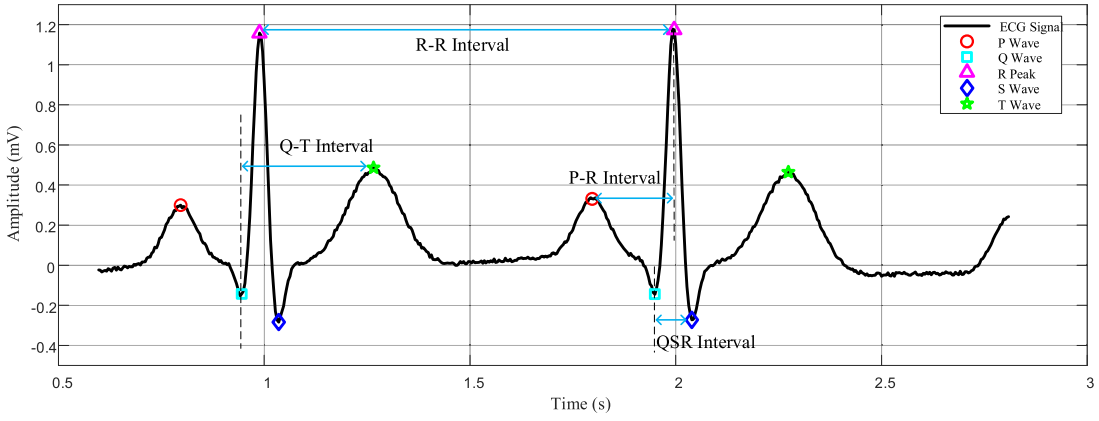

Fig. 9. Schematic of key ECG parameters.

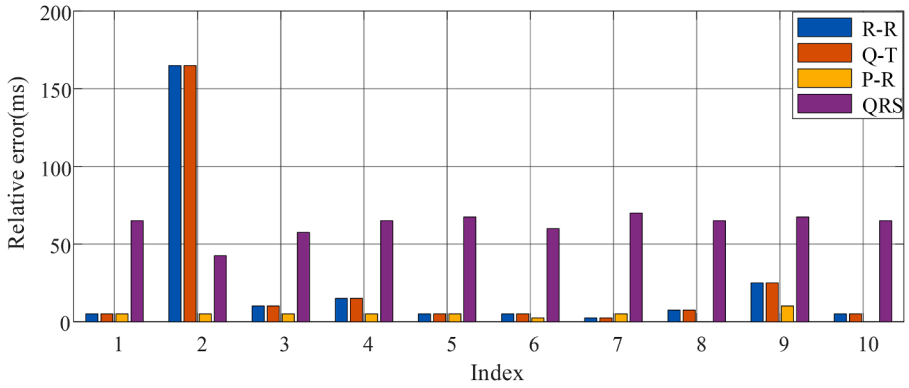

Fig. 10. The R-R Q-T P-R QSR interval error of CNN+LSTM.

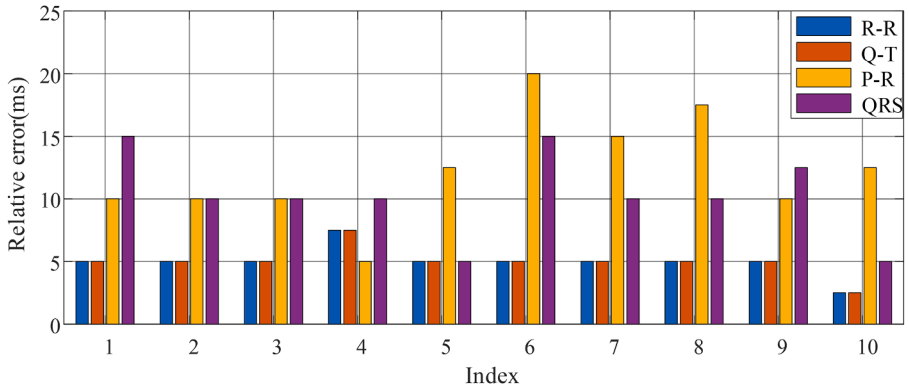

Fig. 11. The R-R Q-T P-R QSR interval error of WaveGRU-net.

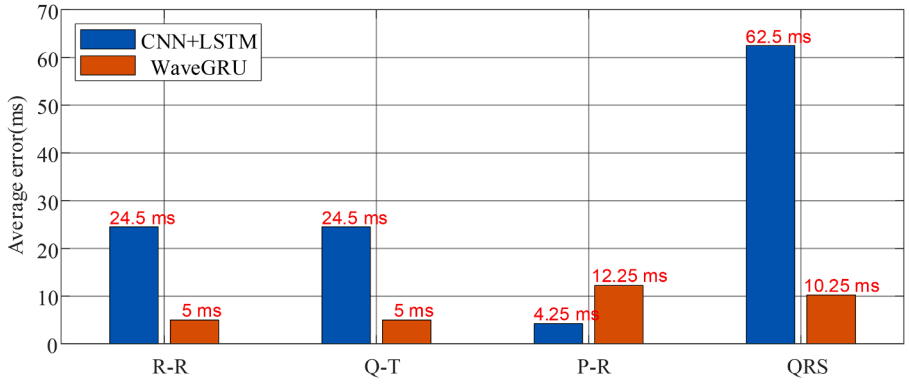

Fig. 12. The R-R Q-T P-R QSR interval mean error of WaveGRU-net and CNN+LSTM.

fluctuations. Fig. 13 presents the evaluation results for RMSSD, SDRR, and pNN50 across the two models, WaveGRU-Net and CNN+LSTM. WaveGRU-Net exhibited smaller fluctuations and greater consistency in RMSSD and SDRR, indicating more stable predictions for heart rate variability with reduced influence from outliers. In contrast, CNN+LSTM showed significantly higher values in these two metrics, especially with greater variability in RMSSD, suggesting that its HRV predictions are less consistent than those of WaveGRU-Net. However, the pNN50 values for both models were nearly zero, indicating that both effectively maintained differences between successive inter-beat intervals within 50 ms, aligning with healthy data collection standards. Overall, WaveGRU-Net demonstrated greater consistency in HRV performance, whereas CNN+LSTM exhibited more variability.

5. Conclusion

This paper proposes a non-contact ECG reconstruction method using millimeter-wave MIMO FMCW radar, integrating multi-scale analysis with a deep learning model for high-precision ECG cardiac signals reconstruction. The system amplifies cardiac signals by capturing phase variations from heart motion. It uses 2D beamforming to enhance heart signals. A cumulative sliding window energy spectrum method is then applied to enhance the SNR. To accurately reconstruct ECG signals, the WaveGRU-Net model is proposed. The model integrates multi-scale decomposition using a MODWT layer, convolutional feature extraction, and a bidirectional GRU module. This design effectively captures complex temporal features in radar reflected signals. Experimental results demonstrate that WaveGRU-Net outperforms the conventional CNN-LSTM model. It reconstructs ECG signals closely aligned with the

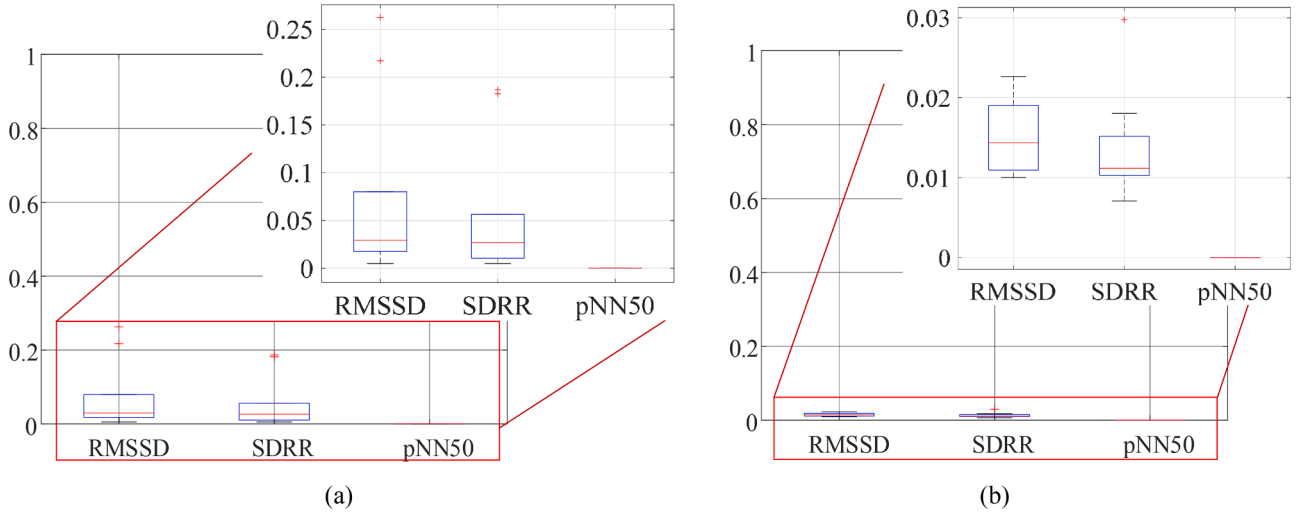

Fig. 13. The RMSSD,SDRR,pNN50 of (a) CNN+LSTM and (b) WaveGRU-net.

real ones. The model achieves lower RMSE, higher PCC, and greater cosine similarity, highlighting its superiority in maintaining morphological consistency. Additionally, error analysis of the four key ECG intervals—P-R, Q-T, QRS, and R-R—confirms that the reconstructed ECG signals achieve high temporal consistency. This study focuses on healthy participants, but future research will involve cardiovascular patients to evaluate clinical applicability. Enhancing real-time performance and computational efficiency will also be crucial for broader medical use. Millimeter-wave radar-based ECG monitoring systems are expected to enable reliable, non-invasive, and long-term cardiac health monitoring.

CRediT authorship contribution statement

Dan Xu: Writing – review & editing, Writing – original draft, Methodology, Formal analysis, Conceptualization. **Yiming Xu:** Writing – review & editing, Writing – original draft, Validation. **Kaijie Xu:** Methodology, Conceptualization. **Ze Hu:** Investigation. **Mengdao Xing:** Supervision, Formal analysis, Conceptualization. **Fulvio Gini:** Writing – review & editing, Methodology, Formal analysis. **Maria Sabrina Greco:** Writing – review & editing, Formal analysis, Conceptualization.

Declaration of competing interest

None.

Acknowledgement

The work of F. Gini and M.S. Greco has been partially supported by the Italian Ministry of Education and Research (MUR) in the framework of the FoReLab project (Departments of Excellence). In addition, we thank Prof. Nicola Vanello from the University of Pisa for providing useful comments that helped improve this article.

Data availability

The authors do not have permission to share data.

References

[1] Z. Fang, P. Jian, H. Zhang, et al., Review of non-contact medical health monitoring technology based on FMCW radar, J. Radars 11 (3) (2022) 499–516.
[2] T. Malapane, W. Doorsamy, B.S. Paul, An intelligent IoT-based health monitoring system, in: Proceedings of the 2020 International Conference on Intelligent Data Science and Technology Applications (IDSTA), Valencia, Spain, 2020, pp. 95–100.
[3] K.M. Chen, Y. Huang, J. Zhang, A. Norman, Microwave life-detection systems for searching human subjects under earthquake rubble or behind barrier, IEEE Transact. Biomed. Eng. 47 (1) (2000) 105–114. Jan.
[4] L. Saikevičius, V. Raudonis, G. Dervinis, V. Baranauskas, Non-contact vision-based techniques of vital sign monitoring: systematic review, Sensors 24 (12) (2024) 3963.
[5] M. Forouzanfar, M. Mabrouk, S. Rajan, M. Bolic, H.R. Dajani, V.Z. Groza, Event recognition for contactless activity monitoring using phase-modulated continuous wave radar, IEEE Transact. Biomed. Eng. 64 (2) (2017) 479–491. Feb.
[6] F. JalaliBidgoli, S. Moghadami, S. Ardalan, A compact portable microwave life-detection device for finding survivors, IEEe Embed. Syst. Lett. 8 (1) (2016) 10–13. Mar.
[7] F. Adib, H. Mao, Z. Kabelac, D. Katabi, R.C. Miller, Smart homes that monitor breathing and heart rate, in: Proceedings of the 33rd Annual ACM Conference on Human Factors in Computing Systems (CHI), 2015, pp. 837–846.
[8] H. Wang, et al., Human respiration detection with commodity WiFi devices: do user location and body orientation matter?, in: Proceedings of the 2016 ACM International Joint Conference on Pervasive and Ubiquitous Computing (UbiComp), 2016, pp. 25–36.
[9] M. Mercuri, et al., Enabling robust radar-based localization and vital signs monitoring in multipath propagation environments, IEEE Transact. Biomed. Eng. 68 (11) (2021) 3228–3240. Nov.
[10] Z. Chen, T. Zheng, C. Cai, J. Luo, MoVi-Fi: motion-robust vital signs waveform recovery via deep interpreted RF sensing, in: Proceedings of the 27th Annual International Conference on Mobile Computing and Networking (ACM MobiCom'21), New Orleans, LA, USA, 2022. Jan.
[11] H.Y. Chang, C.H. Hsu, W.H. Chung, Fast acquisition and accurate vital sign estimation with deep learning-aided weighted scheme using FMCW radar, in: Proceedings of the 2022 IEEE 95th Vehicular Technology Conference (VTC2022-Spring), Helsinki, Finland, 2022, pp. 1–6.
[12] D.M. Bers, Cardiac excitation–contraction coupling, Nature 415 (6868) (2002) 198–205.
[13] V. Gurev, T. Lee, J. Constantino, H. Arevalo, N.A. Trayanova, Models of cardiac electromechanics based on individual hearts imaging data, Biomech. Model. Mechanobiol. 10 (3) (2011) 295–306.
[14] J. Christoph, J. Lebert, Inverse mechano-electrical reconstruction of cardiac excitation wave patterns from mechanical deformation using deep learning, Chaos. 30 (12) (2020).
[15] S. Dong, L. Wen, C. Gu, J. Mao, Contactless detection for heart sounds based on Doppler radar sensor, in: Proceedings of the 2022 IEEE MTT-S International Wireless Symposium (IWS), Harbin, China, 2022, pp. 1–3.
[16] M. Haescher, F. Höpfner, W. Chodan, et al., Transforming seismocardiograms into electrocardiograms by applying convolutional autoencoders, in: Proceedings of ICASSP 2020 –2020 IEEE International Conference on Acoustics, Speech, and Signal Processing (ICASSP), 2020, pp. 4122–4126.
[17] A. Taebi, B.E. Solar, A.J. Bomar, R.H. Sandler, H.A. Mansy, Recent advances in seismocardiography, Vibration. 2 (1) (2019) 64–86.
[18] X. Tian, Q. Zhu, Y. Li, M. Wu, Cross-domain joint dictionary learning for ECG reconstruction from PPG, in: Proceedings of the IEEE International Conference on Acoustics, Speech, and Signal Processing (ICASSP), 2020, pp. 936–940. May.
[19] H.Y. Chiu, H.H. Shuai, P.C.P. Chao, Reconstructing QRS complex from PPG by transformed attentional neural networks, IEEe Sens. J. 20 (20) (2020) 12374–12383. June.
[20] K. Yamamoto, T. Ohtsuki, Non-contact heartbeat detection by heartbeat signal reconstruction based on spectrogram analysis with convolutional LSTM, IEEe Access. 8 (2020) 123603–123613. June.

[21] S. Wu, T. Sakamoto, K. Oishi, T. Sato, K. Inoue, T. Fukuda, et al., Person-specific heart rate estimation with ultra-wideband radar using convolutional neural networks, IEEe Access. 7 (2019) 168484–168494. Nov.
[22] S. Ji, H. Wen, J. Wu, Z. Zhang, K. Zhao, Systematic heartbeat monitoring using an FMCW mm-wave radar, in: Proceedings of the IEEE International Conference on Consumer Electronics and Computer Engineering, 2021, pp. 714–718. Jan.
[23] D. Toda, R. Anzai, K. Ichige, R. Saito, D. Ueki, ECG signal reconstruction using FMCW radar and convolutional neural network, in: Proceedings of the 2021 20th International Symposium on Communications and Information Technologies (ISCIT), Tottori, Japan, 2021, pp. 176–181.
[24] K. Yamamoto, R. Hiromatsu, T. Ohtsuki, ECG signal reconstruction via Doppler sensor by hybrid deep learning model with CNN and LSTM, IEEe Access. 8 (2020) 130551–130560.
[25] Z. Wang, B. Jin, S. Li, F. Zhang, W. Zhang, ECG-grained cardiac monitoring using UWB signals, in: Proceedings of the ACM on Interactive, Mobile, Wearable and Ubiquitous Technologies 6, 2022 186. Art. no.Dec.pages.
[26] S. Dong, Y. Zhang, C. Ma, Q. Lv, C. Li, L. Ran, Cardiogram detection with a millimeter-wave radar sensor, in: Proceedings of the 2020 IEEE Radio and Wireless Symposium (RWS), San Antonio, TX, USA, 2020, pp. 127–129.
[27] S. Ji, et al., RBHHM: A novel remote cardiac cycle detection model based on heartbeat harmonics, Biomed. Signal. Process. Control (2022).
[28] Y.C. Tsai, et al., High accuracy respiration and heart rate detection based on artificial neural network regression, in: Proceedings of the 2020 42nd Annual International Conference of the IEEE Engineering in Medicine & Biology Society (EMBC), Montreal, QC, Canada, 2020, pp. 232–235.
[29] E. Grooby, et al., Neonatal heart and lung sound quality assessment for robust heart and breathing rate estimation for telehealth applications, IEEe J. Biomed. Health Inform. 25 (12) (2021) 4255–4266. Dec.
[30] C.C. Moore, C.H. Lugo-Olivieri, E.R. McVeigh, E.A. Zerhouni, Three-dimensional systolic strain patterns in the normal human left ventricle: characterization with tagged MR imaging, Radiology. 214 (2) (2000) 453–466.
[31] Y. Notomi, et al., Assessment of left ventricular torsional deformation by Doppler tissue imaging: validation study with tagged magnetic resonance imaging, Circulation 111 (9) (2005) 1141–1147.
[32] M.J. Tadi, et al., Gyrocardiography: a new non-invasive monitoring method for the assessment of cardiac mechanics and the estimation of hemodynamic variables, Sci. Rep. 7 (1) (2017) 1–11.
[33] A. Taebi, B.E. Solar, A.J. Bomar, R.H. Sandler, H.A. Mansy, Recent advances in seismocardiography, Vibration. 2 (1) (2019) 64–86.
[34] L. Fulai, L. Haonan, Q. Fugui, A. Qiang, W. Jianqi, Imaging of multiple stationary humans using a UWB MIMO bio-radar, J. Radars 5 (5) (2016) 470–476.
[35] C. Kammer, A. Karimi, Robust distributed averaging frequency control of inverter-based microgrids, in: Proceedings of the 2016 IEEE 55th Conference on Decision and Control (CDC), Las Vegas, NV, USA, 2016, pp. 4973–4978.
[36] L.A. López-Valcárcel, M. García Sánchez, F. Fioranelli, O.A. Krasnov, An MTI-like approach for interference mitigation in FMCW radar systems, IEEE Transact. Aerospace Electron. Syst. 60 (2) (2024) 1985–2000. April.
[37] B. Xue, G. Zhang, F. Gini, M.S. Greco, H. Leung, A high-order motion parameter estimation of moving target for miniature dechirped MMW radar, IEEE Transact. Aerospace Electron. Syst. 60 (6) (2024) 8332–8348. Dec.
[38] Q. Zhou, Y. Yuan, H. Li, Y. Lai, M.S. Greco, F. Gini, W. Yi, Target localization for distributed hybrid active-passive radars, IEEE Transact. Aerospace Electron. Syst. (2025).
[39] G. Dai, S. Huan, L. Zhang, Integrating agile waveforms With DBF for HRWS SAR imagery and adaptive jamming suppression, IEEe J. Sel. Top. Appl. Earth. Obs. Remote Sens. 16 (2023) 4080–4095.
[40] H. Mesa, Adapted wavelets for pattern detection, in: A. Sanfeliu, M.L. Cortés (Eds.), Progress in Pattern Recognition, Image Analysis and Applications, Progress in Pattern Recognition, Image Analysis and Applications, 3773, Springer, Berlin, Heidelberg, 2005, pp. 933–940.
[41] Ma Lele, Kong Xiaobing, Guo Lei, Liu Yuanyan, Liu Xiangjie, Photovoltaic power forecasting based on maximum overlap discrete wavelet transform and deep learning[J], Acta Energ. Solaris Sinica 45 (5) (2024) 576–583.
[42] W. Zhao, Z. Li, J. Hu, Y. Ma, A simple and effective deep neural network based QRS complex detection method on ECG signal, Front. Physiol. 15 (2024) 1384356. Art. no.
[43] A. Shokouhmand, N.D. Aranoff, E. Driggin, et al., Efficient detection of aortic stenosis using morphological characteristics of cardiomechanical signals and heart rate variability parameters, Sci. Rep. 11 (2021) 23817. Art. no.
[44] M. Nosrati, N. Tavassolian, Accurate doppler radar-based cardiopulmonary sensing using chest-wall acceleration, IEEe J. Electromagn. RF. Microw. Med. Biol. 3 (1) (2019) 41–47. Mar.
[45] J. Yun, H. Mengxue, Z. Junming, et al., Monitoring of human vital signs by millimeter wave radar: a Meta-analysis, Chin. J. Convalescent Med. 34 (2) (2025) 62–69.
[46] U. Ssumalatha, K.K. Prakasha, S. Prabhu, V.C. Nayak, Deep learning applications in ECG analysis and disease detection: an investigation study of recent advances, IEEe Access. 12 (2024) 126258–126284.